Journal Name

ARTICLE

Controllable rotational inversion in nanostructures with dual chirality

Received 00th January 20xx,
Accepted 00th January 20xx

DOI: 10.1039/x0xx00000x

www.rsc.org/

Lu Dai,*[a,e] Ka-Di Zhu,[b] Wenzhong Shen,[b] Xiaojiang Huang,[c] Li Zhang,*[d] Alain Goriely[e]

Chiral structures play an important role in natural sciences due to their great variety and potential applications. A perversion connecting two helices with opposite chirality creates a dual-chirality helical structure. In this paper, we develop a novel model to explore quantitatively the mechanical behavior of normal, binormal and transversely isotropic helical structures with dual chirality and apply these ideas to known nanostructures. It is found that both direction and amplitude of rotation can be finely controlled by designing the cross-sectional shape. A peculiar rotational inversion of overwinding followed by unwinding, observed in some gourd and cucumber tendril perversions, not only exists in transversely isotropic dual-chirality helical nanobelts, but also in the binormal/normal ones when the cross-sectional aspect ratio is close to 1. Beyond this rotational inversion region, the binormal and normal dual-chirality helical nanobelts exhibit a fixed directional rotation of unwinding and overwinding, respectively. Moreover, in the binormal case, the rotation of these helical nanobelts is nearly linear, which is promising as a possible design for linear-to-rotary motion converters. The present work suggests new designs for nanoscale devices.

Introduction

Chiral structures play a prominent role in many natural and technology processes ranging from protein configuration,[1,2] development, to nanomechanics.[3,4] Helices with given chirality are critical elements in a host of applications at the nanoscale as they provide simple springs and, more importantly, a direct way to convert linear motion to rotational motion and rotational motion to linear motion. An example of this conversion process is the functionalized helical micro-/nano-swimmers, which are optimized to have a pure rotation translation along their helical axis.[5] Such swimming robots are a promising tool for single-cell-targeted drug, DNA, and enzymes delivery in vitro as well as in vivo.[6-8] Conversely, in the transformation from linear motion to rotational motion, elasticity plays a key role. Yet, the linear regime of simple springs is limited due to torsional lock-up: as a spring is pulled in simple extension, it quickly stiffens due to its inability to untwist without one of the end turning. An elegant solution to this mechanical problem, first proposed in ref. (9), is to design a "twistless spring" by using filaments that exhibit both left and right chirality connected by a short inversion called a "perversion", a term introduced by the mathematician J.B. Listing to describe the reversal of one chiral structure into another.[10]

This kind of helices with dual chirality was first described in plant physiology in a letter of André-Marie Ampère.[11,12] Then Charles Darwin pointed out that a tendril with perversion creates a twistless flexible elastic structure connecting a climbing plant to its support[13] (see ref. (14) for historical details). Inspired by the tendrils, it is found that an inverted structure can be created through an instability in a filament with intrinsic curvature under tension by either decreasing the tension or increasing the intrinsic curvature.[15] The structure emerging has dual chirality and, due to its particular cancellation of twist, has an excellent mechanical behavior of tension-extension close to an ideal linear Hookean response.[9] Moreover, a helical structure with dual chirality has a remarkable rotational property during extension: It is reported that some young and old cucumber tendril coils unwinds and overwinds with axial extension, respectively.[16]

There is yet another peculiar rotational behavior of helices with dual chirality. As presented in Fig. 1(a), we find that some young gourd and cucumber tendrils, always overwind in the beginning of axial extension, and then unwind when elongation is further increased (ESI Movie S1† for gourd and ESI Movie S2† for cucumber). In this experiments, we use a slow axial loading (of about 0.3cm/s, 0.05 coil length per second) so that the tendril is in a quasi-static equilibrium for all times. Fig. 1(b) displays the rotation states of a gourd tendril coil during axial loading. The gourd tendril coil first overwinds

[a] School of Mathematics and Physics, Suzhou University of Science and Technology, Suzhou 215009, China.
E-mail: dailu.1106@aliyun.com
[b] Department of Physics and Astronomy, Shanghai Jiao Tong University, 800 Dongchuan Road. Minhang District, Shanghai 200240, China
[c] College of Science, Donghua University, Shanghai 201620, China
[d] Department of Mechanical and Automation Engineering, The Chinese University of Hong Kong, Shatin NT, Hong Kong SAR, China.
E-mail: lizhang@mae.cuhk.edu.hk
[e] Mathematical Institute, University of Oxford, Oxford OX2 6GG, United Kingdom
†Electronic Supplementary Information (ESI) available. See DOI: 10.1039/x0xx00000x

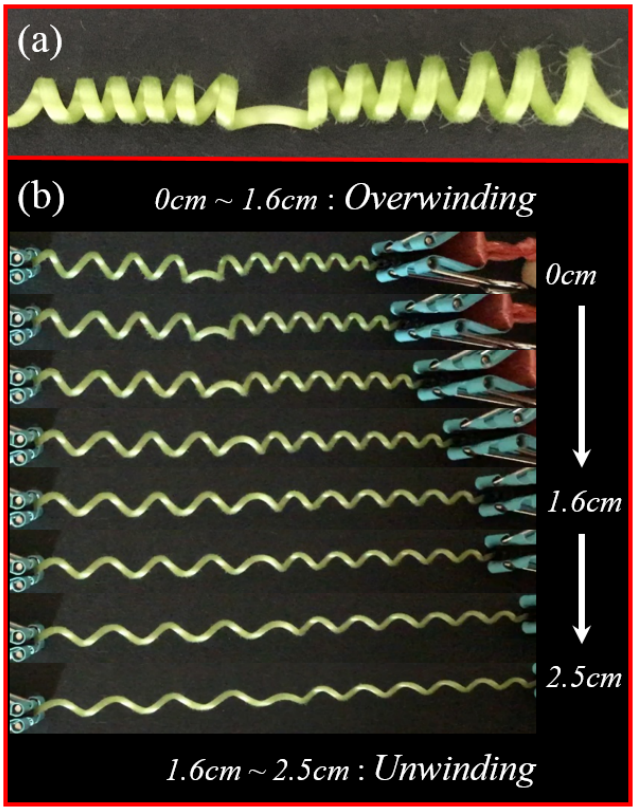

Fig.1 (a) A gourd tendril coil. (b) The rotation states of a gourd tendril coil during an axial loading process.

when the elongation increases to 1.6cm, and then unwinds in the rest of the loading process. Interestingly, this non-monotonic behavior, known as the twist-stretch coupling, also exists in the microscopic single-chirality DNA molecules.[17,18] As extension increases, each point on the DNA rotates around the axis by first overwinding around it (adding further twist in the spring) then unwinding it (hence removing twist).[19,20]

Helical rods can be classified into three types: *transversely isotropic helices* (with rotationally invariant sections such as squares and circles), and *normal and binormal helices* with non-rotational invariant section (such as rectangle or elliptical cross sections).[21] In this paper, we study the rotational and extensional behaviour of nanohelices with dual chirality that have either transverse isotropy or are composed of normal and binormal helices (referred to here as "nanobelts"). A binormal dual-chirality nanobelt can be fabricated via strain-driven self-rolling mechanism.[22] These structures are known to unwind during axial extension.[23] A normal dual-chirality nanobelt can be realized by 3D direct laser writing, which has been used to print single normal nanohelices.[24] A transversely isotropic cellulosic micro/nano-fiber with dual-chirality can be produced by electrospinning in liquid crystalline solutions.[25] Under electronic beam exposure, a suspended cellulosic fiber exhibits unwinding and overwinding behavior.[26] Therefore, it is of great practical significance to provide an accurate theoretical description of the mechanical properties for the normal, binormal, and isotropic dual-chirality nanohelices.

In this paper, we provide a theoretical basis for the mechanics of normal, binormal, and transversely isotropic helical nanostructures with dual chirality by employing a general extensible rod theory. We show that by modifying the shape of the cross-section, one can tune the rotational properties of direction and amplitude of these structures to obtain a linear rotational response under extension. In particular, a controllable rotational inversion can be obtained from the dual-chirality nanohelices of transversely isotropy, as well as of normal/binormal in a narrow region defined by the aspect ratio of rectangular cross-section.

Modeling

The general set-up of our model is shown in Fig. 2(a)-(d). We assume that a rod with width w and thickness t ($w > t$) rolls up into a uniform helical structure with dual chirality H_{PI}, with radius a_0, pitch b_0, and N_0 helical turns. This structure is slowly loaded by an axial force F , while the ends are prevented from rotating. In this process, the structure is transformed into another helical structure with dual chirality H_{PF}, with radius a, pitch b, and N helical turns. The director basis $\boldsymbol{D}_i$ (i = 1, 2, 3) consisting of the normal, binormal, and tangent vectors of H_{PI} and the director basis $\boldsymbol{d}_i$ of H_{PF} are described by their Euler angles (φ_0, ϑ_0, ψ_0) and (φ, ϑ, ψ), respectively.[27, 28] We can use the mirror symmetry of these structures to our advantage by modeling their response as two helical springs where one end is free to rotate. We follow the terminology of ref. (29) and denote S to be the arc length along the fixed reference configuration H_{PI} and s the arc length along the deformed configuration H_{PF}. The corresponding derivatives are defined by $\widehat{(\cdot)} = \partial(\cdot)/\partial S$ and $\dot{(\cdot)} = \partial(\cdot)/\partial s$. Based on the general elastic rod theory, the derivation processes for the radii a_0 and a, pitches b_0 and b as well as the loading force F, the torque along the helix axis M of each helix of H_{PF} are the same as that

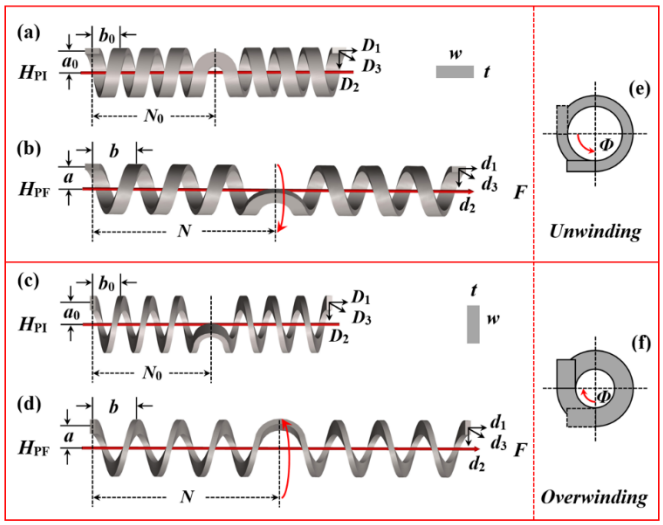

Fig.2 Schematic illustration of the dual-chirality nanohelices with rectangular cross-section H_{PI} of (a) binormal and (c) normal. Configurations of the corresponding elongated nanohelix with dual chirality H_{PF} of (b) binormal and (d) normal after loading by the tensile force F along helical axes. The corresponding cross sections of the whole (e) binormal and (f) normal nanohelices with dual chirality at the mirror symmetry axes.

of a loaded helical structure with two ends restricted from winding,[29] except that in this situation $\hat{\psi} \neq \dot{\psi}_0$ due to the fact that $N \neq N_0$. Therefore, the radius and pitch are given by:

$$a_0 = \frac{\sin\theta_0}{\dot{\psi}_0},\ b_0 = \frac{2\pi\cos\theta_0}{\dot{\psi}_0}, \tag{1}$$

$$a = \frac{1}{\hat{\psi}}\left[\left(\frac{F}{E_3}\cos\theta + 1\right) - \frac{F}{E_1}\cos\theta\right]\sin\theta,$$

$$b = \frac{2\pi}{\hat{\psi}}\left[\frac{F}{E_1}\sin^2\theta + \left(\frac{F}{E_3}\cos\theta + 1\right)\cos\theta\right]. \tag{2}$$

For a helix with N helical turns of H_{PF}, the number of turns N is given by:[30]

$$N = \frac{\hat{\psi}}{2\pi} l_0, \tag{3}$$

where $l_0 = N_0\sqrt{(2\pi a_0)^2 + b_0^2}$ is the length of coil wire of H_{PI}.

The balance of force and moment connect the axial force F and axial moment M to the deformed shape of the helical structure by the following two relations:

$$\left(\frac{1}{E_3} - \frac{1}{E_1}\right)\cos\theta\sin\theta F^2 + \sin\theta F - C\left(\hat{\psi}\cos\theta - \dot{\psi}_0\cos\theta_0\right)\hat{\psi}\sin\theta + EI_1\left[1 - (1-\Delta)\delta_{i2}\right]\left(\hat{\psi}\sin\theta - \dot{\psi}_0\sin\theta_0\right)\hat{\psi}\cos\theta = 0, \tag{4}$$

$$M = EI_1\left[1 - (1-\Delta)\delta_{i2}\right]\left(\hat{\psi}\sin\theta - \overset{g}{\psi}_0\sin\theta_0\right)\sin\theta + C\left(\hat{\psi}\cos\theta - \overset{g}{\psi}_0\cos\theta_0\right)\cos\theta, \tag{5}$$

where $\Delta \equiv I_2/I_1$, i = 1 for a normal (i = 2 for a binormal) helix and $I_1 = w^3t/12$, $I_2 = wt^3/12$ are the moment of inertia of a rectangular cross section. δ_{i2} is the Kronecker delta. $E_1 = KGtw$, $E_3 = Etw$ and $C = 4GI_1I_2/(I_1+I_2)$ according to the scaled torsional stiffness.[31] K is the Timoshenko shear coefficients and related to the Poisson's ratio ν through $K = (5+5\nu)/(6+5\nu)$.[32] E and $G = E/2(1+\nu)$ are the Young's and shear moduli of the material, respectively.[33]

It is of particular interest to look at the case M=0 for a loaded helical structure, corresponding to the case where one end is free to rotate. From (4), we obtain

$$\hat{\psi} = \frac{EI_1\left[1 - (1-\Delta)\delta_{i2}\right]\sin\theta_0\sin\theta + C\cos\theta_0\cos\theta}{EI_1\left[1 - (1-\Delta)\delta_{i2}\right]\sin^2\theta + C\cos^2\theta}\overset{g}{\psi}_0. \tag{6}$$

Fig. 2(e) and 2(f) are the cross sections of the binormal and normal helical structures with dual chirality at the mirror symmetry axes, respectively. The perversions before and after loading are presented by the solid and dashed rectangles, respectively. Φ is the rotation angle of the free end of helical structure, *i.e.*, the rotation angle of perversion:

$$\Phi = 360^\circ \times (N - N_0). \tag{7}$$

The spring constant of each helical structure of H_{PF} is deduced from (1)-(4), in the linear limit $h = dF/d(Nb)$:

$$h_S = -\frac{P_1P_3}{2(P_1P_4 + P_2)},$$

$$P_1 = \left(\frac{1}{E_3} - \frac{1}{E_1}\right)\left(\sin\theta - \frac{\cos^2\theta}{\sin\theta}\right)F^2 - \frac{\cos\theta}{\sin\theta}F + \frac{Q_6}{2\cos\theta}\left(\sin\theta - \frac{\cos^2\theta}{\sin\theta}\right)\hat{\psi}^2 + \left[2\sin\theta\frac{Q_6(Q_4Q_5 + Q_3Q_6)}{Q_4^2} - \frac{Q_3}{\sin\theta}\right]\dot{\psi}_0\hat{\psi} + \sin\theta\frac{Q_5(Q_4Q_5 + Q_3Q_6)}{Q_4^2}\dot{\psi}_0^2$$

$$P_2 = Q_2\sin\theta,\ P_3 = \frac{1}{Q_2l_0},\ P_4 = -\frac{Q_1}{Q_2},$$

where,

$$Q_1 = \left(\frac{1}{E_3} - \frac{1}{E_1}\right)\cos^2\theta + \frac{1}{E_1},\ Q_2 = 2\left(\frac{1}{E_3} - \frac{1}{E_1}\right)F\cos\theta + 1,$$

$$Q_3 = EI_1\left[1 - (1-\Delta)\delta_{i2}\right]\sin\theta_0\sin\theta + C\cos\theta_0\cos\theta,$$

$$Q_4 = EI_1\left[1 - (1-\Delta)\delta_{i2}\right]\sin^2\theta + C\cos^2\theta,$$

$$Q_5 = -EI_1\left[1 - (1-\Delta)\delta_{i2}\right]\sin\theta_0\frac{\cos\theta}{\sin\theta} + C\cos\theta_0,$$

$$Q_6 = 2\left(EI_1\left[1 - (1-\Delta)\delta_{i2}\right] - C\right)\cos\theta, \tag{8}$$

Since the two opposite-handed helical structures of H_{PF} are connected in series, the spring constant of H_{PF} is:

$$h_P = \frac{h_S}{2}. \tag{9}$$

Using (1)-(9), we can obtain the radius a, pitch b, N helical turns and the spring constant h_P of the helical structure with dual chirality H_{PF} from the known radius a_0, pitch b_0, number of turns in each helix N_0 of H_{PI} and the loading force F.

Results

In order to understand the mechanical behavior of nanohelices with dual chirality, we analyze a rolled up nanohelix. The strain-induced self-scrolling mechanism is a highly controllable fabrication method that allows to create dual-chirality nanohelices with adjustable helix angles. Fig. 3(a) shows that a binormal dual-chirality nanohelix are fabricated from the symmetric V-shaped SiGe/Si/Cr nanobelt, which leads to a left and right-handed arm having the same geometry parameters. The 8/10 nm thick SiGe/Si hetero-structures with approximately 40% Ge in the SiGe layer were epi-grown by chemical vapor deposition (CVD) on the Si(110) substrates. The 13 nm thick amorphous Cr layers were deposited by e-beam evaporation. Details of the SiGe/Si/Cr pattern fabrication and the wet chemical etching for the subsequent underetching

were described elsewhere.[22,34] The binormal nanohelix with dual chirality has radius a_0=1.18μm, pitch b_0=4.47μm and N_0=6. The insets present the V-shaped mesa designs of 60°, as well as the rolling direction of the helix as indicated with a white arrow. In the following calculation, we use the parameters of this fabricated SiGe/Si/Cr nanohelix, including the area of the cross-section, the radius, the pitch, the number of turns, and the material parameters. (As presented in ESI Fig. S1, we provide another SiGe/Si/Cr binormal dual-chirality nanohelix as an example to quantitatively analyse the mechanical properties of rotation.)

By pulling both ends of a nanohelix with dual chirality, the central part of the perversion performs a rotary motion,[16,23] which makes it a perfect material for a linear-to-rotary motion nanometer converter. Fig. 3(b) presents the rotation angle of perversion versus the axial elongation for the fabricated binormal SiGe/Si/Cr nanohelix with the red curve. The modeling results are deduced from (1)-(6) with the geometry parameters as well as the material parameters of E_{SiGe}=161.2GPa, v_{SiGe}=0.27[34] E_{Si}=168.9GPa, v_{Si}=0.36,[35,36] E_{Cr}=377GPa, v_{Cr}=0.31.[37] The SiGe/Si/Cr binormal nanohelix unwinds while extending axially and rotates 358˚, *ca.* 1 turn, when it is stretched to 160% of its original length. The unwinding rotation direction of this binormal nanohelix is marked by red arrows in Fig. 2(b) and 2(e). Remarkably, during the first turn, the rotation angle and the axial elongation are very close to a linear relation and the corresponding linear-to-rotary ratio is approximately 597˚ per unit length. This kind of linear rotation has been observed in a loading experiment of SiGe/Si nanohelix.[23] As shown in Fig.3(b), we also study the linear-to-rotary motion of a normal dual-chirality helical nanohelix with the same parameters as those of the binormal SiGe/Si/Cr nanohelix. It is interesting to compare the binormal and normal nanohelices. The normal helix overwinds in the reverse direction and has a larger amplitude of rotation: it overwinds to 1116˚, *i.e.* 3.1 turns, when the elongation reaches 60% (see Fig. 2(d) and 2(f)). It is notable that the normal helix deviates from a linear behavior in the elastic regime by only 10%. Therefore, the binormal nanohelices with dual chirality are a more appropriate choice for a linear-to-rotary motion nanometer converter in 3-D scanning probe microscopes or microgoniometers.

Fig. 3(c) illustrates the axial load versus elongation of the SiGe/Si/Cr binormal nanohelix with dual chirality and the corresponding normal helix in the region of 60% elongation, using (1)-(6). All the loading forces of binormal/normal nanohelices are divided by their respective maximum loading force in this region. We observe that the binormal nanohelix with dual chirality is stretched linearly with the loading force, unlike the normal helix.

We further describe in Fig. 3(d) how the spring constant depends on the elongation for both the SiGe/Si/Cr binormal and normal nanohelices with dual chirality in the region of 60% elongation, obtained using (7) and (8). The spring constant of binormal nanohelix remains constant with a value of 0.012N/m, which will facilitate the actuation of the motion converters. A spring constant of the same magnitude of order as 0.012N/m has been measured in a SiGe/Si nanohelix.[23] In contrast, the normal nanohelix has a wide spring constant change from 0.014N/m to 0.379 N/m, increasing 27 times under load. Therefore, we conclude that the binormal nanohelices with dual chirality is more appropriate for high-resolution force measurement in nanoelectromechanical systems.

Since normal and binormal helices exhibit opposite rotary motions, what is the behavior of a transversely isotropic rod (created with a square or circular section)? Fig. 4(a) presents the rotation angle Φ of perversion versus the axial elongation for a transversely isotropic dual-chirality nanohelix with square cross-section, derived from (1)-(7). In the loading process,

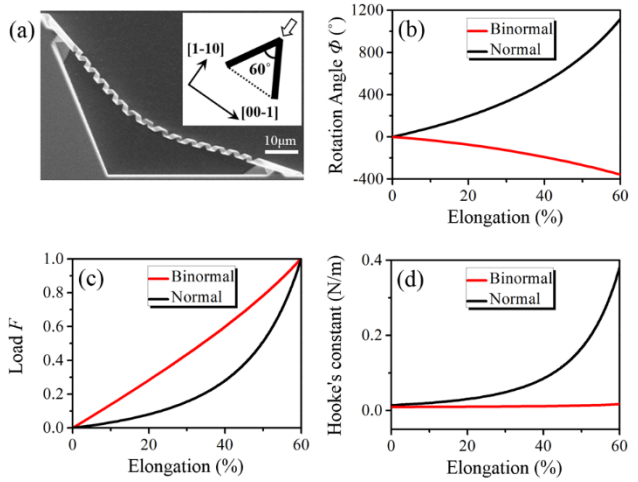

Fig.3 (a) SEM image of a binormal SiGe/Si/Cr dual-chirality helical nanohelix formed by a symmetric V-shaped mesa with both ends fixed to the Si(110) substrate. The inset shows the mesa design and the rolling direction of the helix as indicated with a hollow arrow. (b) Rotation angle of perversion, (c) axial load, (d) spring constant versus axial elongation for the fabricated binormal nanohelix as well as a normal one with the same parameters.

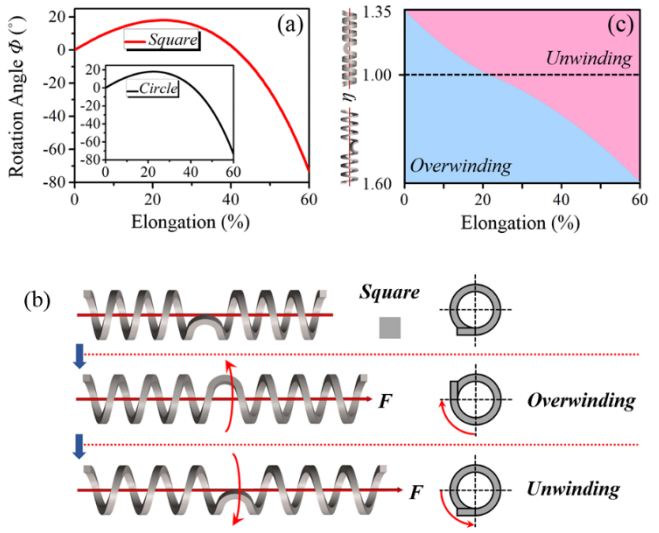

Fig.4 (a) Rotation angle Φ of perversion versus axial elongation for the transversely isotropy dual-chirality nanohelices with square and circle cross-sections. (b) The rotational inversion process of a transversely isotropy dual-chirality nanohelix with square cross-section, as well as its cross-section at the mirror symmetry axis. (c) The rotational inversion region defined by the aspect ratio of rectangular cross-section η.

the dual-chirality nanohelix with square cross-section exhibits the rotational inversion: it first overwinds to 18˚, *i.e.* 0.05 turn, when the elongation increases to 22%; then unwinds to 73˚, *i.e.* 0.2 turn, when the elongation increases to 60% as shown in Fig. 4. Therefore, the rotation property of transversely isotropy dual-chirality nanohelices is displayed in different stages with different axial loads. Interestingly, this rotational inversion is similar to the one we observed in some gourd and cucumber tendrils (Fig. 1(b)). We note that all transversely isotropic rods will behave, as expected from the general theory and illustrated for a fabricated SiGe/Si/Cr nanohelix transforms with a circular cross section (inset of Fig. 4(a)).

We further identify the range of the aspect ratio of rectangular cross-section $\eta=w/t$ for the nanohelices with dual chirality that acquires the characteristic of rotational inversion. Fig. 4 (c) shows how the rotation direction of perversion depends on η during the axial loading, based on (1)-(6). The dashed line of $\eta=1$ represents the dual-chirality nanohelix with square cross-section. The areas above and below the dashed line indicate the binormal and normal helical nanohelices with dual chirality respectively. We note that the rotational inversion of overwinding followed by unwinding only happens in a very narrow region of $1<\eta<1.35$ for binormal nanohelix with dual chirality and $1<\eta<1.6$ for normal one.

Fig. 5 illustrates the rotation angle versus the elongation for 1≤η≤50. The area between two red dotted dashed curves of η=1.35 and η=1.6 is the region of rotational inversion as shown in Fig. 5(b); while the rest is the region of uni-directional rotation. A binormal dual-chirality nanohelix with η≥1.35 or a normal one with η≥1.6 will only unwinds or winds, respectively, during the whole loading process. According to the colourmap, the uni-directional rotation behavior of perversion is affected significantly by the aspect ratio η when it is smaller than 10: for an elongation of 60%, the rotation angle varies from 186° to 352° with η increasing from 1.35 to 10 (binormal), and from 198° to 1049° with η increasing from 1.6 to 10 (normal). However, when the value of η exceeds 10, the relationship between the elongation and rotation angle is close to linear for the binormal nanohelices with dual chirality. We see from this analysis that both direction and amplitude of rotation can be finely adjusted by changing the shape of cross-section for a dual-chirality helical micro-/nano-structure made out of determined material.

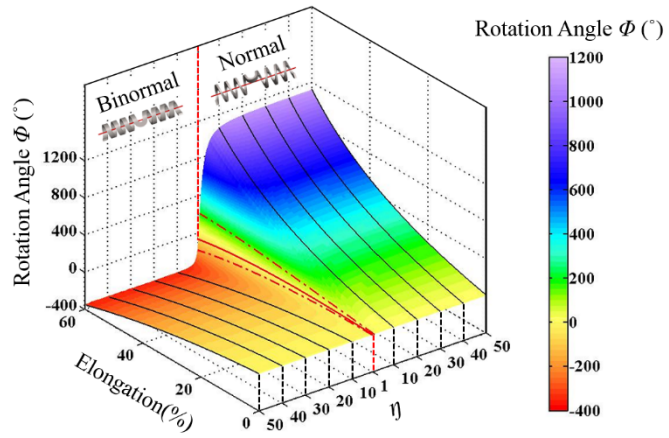

Fig.5 Rotation angle perversion versus elongation for 1≤η≤50.

Conclusions

We have shed light on important mechanical properties of helical nanostructures with dual chirality by using a general elastic rod theory that include bending, torsion, twist, extension, and shear. Our model was used to analyze the behavior of a SiGe/Si/Cr dual-chirality nanohelix. It reveals that the transversely isotropic nanohelix always overwinds initially in axial extension, and then unwinds for larger tension. We also observe that this kind of rotational inversion exists in some gourd and cucumber tendrils. Importantly, we find that a rotational inversion region defined by the aspect ratio of rectangular cross-sections η is given: $1<\eta<1.35$ and $1<\eta<1.6$ for binormal and normal nanohelices with dual chirality, respectively. Beyond this narrow region, the binormal and normal nanohelices with dual chirality only unwinds and overwinds, respectively. It is found that for the normal dual chirality nanohelices, the rotation angle of perversion, loading force and spring constant all increase substantially and nonlinearly with extension. While binormal dual chirality nanohelices with $\eta>10$ rotate and stretch both linearly with loading force, and a spring constant for $\eta=50$ as small as 0.012N/m. Therefore, these remarkable mechanical properties suggest that binormal nanohelices with dual chirality would be excellent linear-to-rotary motion converters. This work provides a theoretical framework for further experimental investigation on helical structures with dual chirality, as well as their applications in novel helical devices and micro-/nano-electromechanical systems.

Conflicts of interest

There are no conflicts to declare.

Acknowledgements

This work was supported by the National Natural Science Foundation of China under Grant No. 11547042, and L.Z. thanks the financial support, by the Early Career Scheme (ECS) with the Project No. 439113, from the Research Grants Council (RGC) of Hong Kong SAR. We thank Qianqian Wang (The Chinese University of Hong Kong) for simulated three-dimensional helices.

References

1 P. Cluzel, A. Lebrun, C. Heller, R. Lavery, J. L. Viovy, D. Chatenay and F. Caron, *Science*, 1996, **271**, 792-794.
2 B. L. Feringa, R. A. Delden, *Angew. Chem. Int. Ed.*, 1999, **38**, 3418-3438.
3 R. Dreyfus, J. Baudry, M. L. Roper, M. Fermigier, H. A. Stone, J. Bibette, *Nature*, 2005, **437**, 862-865.

4 M. G. L. van den Heuvel, C. Dekker, *Science*, 2007, **317**, 333-336.
5 L. Zhang, J. J. Abbott, L.X. Dong, K. E. Peyer, B. E. Kratochvil, H. X. Zhang, C. Bergeles, B. J. Nelson, *Nano Lett.*, 2009, **9**, 3663-3667.
6 S. Tottori, L. Zhang, F. Qiu, K. K. Krawczyk, A. F. Obregón, B. J. Nelson, *Adv. Mater.*, 2012, **24**, 811-816.
7 S. Tottori, L. Zhang, K. E. Peyer and B. J. Nelson, *Nano Lett.*, 2013, **13**, 4263-4268.
8 F. M. Qiu, S. Fujita, R. Mhanna, L. Zhang, B. R. Simona, B. J. Nelson, *Adv. Funct. Mater.*, 2015, **25**, 1666-1671.
9 T. McMillen, A. Goriely, *J. Nonlinear Sci.*, 2002, **12**, 241-281.
10 J. B. Listing, *Vorstudien über topologie*, Göttinger Studien, 1847, I:811-875.
11 A. P. Candolle, *Organographie végétale*. Chez Deterville, Paris, 1827.
12 A. P. Candolle, *Physiologie végétale*. Béchet Jeune, Paris, 1832.
13 Ch. Darwin, *The movements and habits of climbing plants*, John Murray, London, 1865.
14 A. Goriely, The mathematics and mechanics of biological growth, Springer New York, 2017.
15 A. Goriely, M. Tabor, *Phys. Rev. Lett.*, 1998, **80**, 1564-1567.
16 S. J. Gerbode, J. R. Puzey, A. G. McCormick, L. Mahadevan, *Science*, 2012, **337**, 1087-1091.
17 J. Gore, Z. Bryant, M. Nollmann, M. U. Le, N. R. Cozzarelli, C. Bustamante, *Nature*, 2006, **442**, 836-839.
18 T. Lionnet, S. Joubaud, R. Lavery, D. Bensimon, V. Croquette, *Phys. Rev. Lett.*, 2006, **96**, 178102(1-4).
19 J. W. Miller, *Physical Review*, 1902, **14**, 129-148.
20 B. Durickovic, A. Goriely, J. H. Maddocks, *Phys. Rev. Lett.*, 2013, **111**, 108103 (1-5).
21 A. Goriely, P. Shipman, *Phys. Rev. E*, 2000, **61**, 4508-4517.
22 L. Zhang, E. Deckhardt, A. Weber, C. Schonenberger, D. Grutzmacher, *Nanotechnology*, 2005, **16**, 655-663.
23 L. X. Dong, L. Zhang, B. E. Kratochvil, K. Shou, B. J. Nelson, *JMEMS*, 2009, **18**, 1047-1053.
24 T. Y. Huang, M. S. Sakar, A. Mao, A. J. Petruska, F. Qiu, X. B. Chen, S. Kennedy, D. Mooney, B. J. Nelson, *Adv. Mater.*, 2015, **27**, 6644-6650.
25 M. H. Godinho, J. P. Canejo, G. Feioa, E. M. Terentjev, *Soft Matter*, 2010, **6**, 5965-5970.
26 J. P. Canejo, M. H. Godinho, *Materials*, 2013, **6**, 1377-1390.
27 A. Goriely, M. Tabor, *Physica D*, 1997, **160**, 22-44.
28 A. B. Whitman, C. N. Desilva, *J. Elasticity*, 1974, **4**, 265-280.
29 L. Dai, L. Zhang, L. X. Dong, W. Z. Shen, X. B. Zhang, Z. Z. Ye, B. J. Nelson, *Nanoscale*, 2011, **3**, 4301-4306.
30 A. Goriely, M. Tabor, *Proc. Roy. Soc. London Ser. A*, 1997, **453**, 2583-2601.
31 Z. C. Zhou, P. Y. Lai, B. Joos, *Phys. Rev. E*, 2005, **71**, 052801(1-4).
32 W. A. Fate, *J. Appl. Phys.*, 1975, **46**, 2375-2377.
33 S. P. Timoshenko, J. M. Gere, *Mechanics of Materials*, Van Nostrand, Princeton, 1972.
34 L. Zhang, E. Ruh, D. Grutzmacher, L. X. Dong, D. J. Bell, B. J. Nelson, C. Schonenberger, *Nano Lett.*, 2006, **6**, 1311-1317.
35 X. L. Li, *J. Phys. D: Appl. Phys.*, 2008, **41**, 193001(1-12).
36 J. J. Wortman, R. A. Evans, *J. Appl. Phys.*, 1965, **36**, 153-156.
37 S. V. Golod, V. Ya. Prinz, P. Wägli, L. Zhang, O. Kirfel, E. Deckhardt, F. Glaus, C. David, D. Grützmacher, *Appl. Phys. Lett.*, 2004, **84**, 3391-3393.